Late Cretaceous bird from Madagascar reveals novel development of beaks

Patrick M. O'Connor[1,2,3,*], Alan H. Turner[4], Joseph R. Groenke[1], Ryan N. Felice[5], Raymond R. Rogers[3,6], David W. Krause[3,4], & Lydia J. Rahantarisoa[7].

[1]Department of Biomedical Sciences, Heritage College of Osteopathic Medicine, Ohio University, Athens, Ohio 45701, USA.

[2]Ohio Center for Ecology and Evolutionary Studies, Ohio University, Athens, Ohio 45701 USA.

[3]Department of Earth Sciences, Denver Museum of Nature & Science, Denver, Colorado 80205, USA.

[4]Department of Anatomical Sciences, Stony Brook University, Stony Brook, New York 11794, USA.

[5]Centre for Integrative Anatomy, Department of Cell and Developmental Biology, University College London, London, WC1E 6AP, United Kingdom.

[6]Geology Department, Macalester College, 1600 Grand Avenue, St. Paul, Minnesota 55105, USA.

[7]Département de Sciences de la Terre et de l'Environnement, Université d'Antananarivo, Antananarivo (101), Madagascar.

Mesozoic birds display striking differences in size, flight adaptations, and feather organization[1–4], but exhibit relatively conserved patterns of beak shape and development[5–7]. Neornithine (= crown group) birds exhibit constraint on facial development[8–9] as well, but also comparatively diverse beak morphologies associated with a range of feeding and behavioral ecologies. Here we report a new, crow-sized stem bird, *Falcatakely forsterae* gen. et sp. nov., from the Late Cretaceous of Madagascar that possesses a remarkably long and deep rostrum, a novel expression of beak morphology previously unknown among Mesozoic birds and superficially similar to that of a variety of crown group birds (e.g., toucans). The rostrum of *Falcatakely* is composed of an expansive edentulous maxilla and a small tooth-bearing premaxilla. Morphometric analyses of individual bony elements and three-dimensional rostrum shape reveal the development of neornithine-like facial anatomy despite the retention of maxilla-premaxilla organization similar to that of nonavialan theropods. The unique patterning and increased height of the rostrum in *Falcatakely* reveals a degree of developmental lability and increased morphological disparity unknown in early-branching avialans. Expression of this novel phenotype (and presumed ecology) within a stem bird underscores that consolidation to the neornithine-like premaxilla-dominated rostrum was not an evolutionary prerequisite for beak enlargement.

Understanding of Mesozoic bird evolution continues to improve, driven predominantly by discoveries from the Early Cretaceous of China[1–3,6]. Although these specimens exhibit striking variation in body size, soft-tissue anatomy, and inferred ecologies[2–4,10,11], disparity in Mesozoic avialan cranial shape remains restricted to a relatively limited number of forms considered to be either generalists or substrate-probing specialists[5,6,12–15] only distantly related to crown birds. The Late Cretaceous (~100–66 Myr ago) chapter of avialan evolution remains relatively incomplete owing to a paucity of new fossil discoveries (although see recent works on birds such as *Ichthyornis*[16] and *Asteriornis*[17]). Thus, new fossils of Late Cretaceous birds are essential for refining hypotheses relating to avialan morphological evolution and diversification.

The phylogenetic diversity of early branching (non-neornithine) Mesozoic birds is dominated by enantiornithines, heralded as the first avialan diversification and characterized by a range of body sizes and inferred habits[2,14,18–21]. This radiation is notable for its apparent near-global distribution throughout most of the Cretaceous. An exceptionally well-preserved partial cranium of a previously unknown enantiornithine (University of Antananarivo [UA] 10015) from the latest Cretaceous (Maastrichtian) of Madagascar falls within a critical temporal-spatial gap (i.e., the entire Cretaceous of Afro-Madagascar, for which very few avialans are known). The specimen expands our knowledge of realized cranial shape disparity, in terms of both morphological details and proportions of elements, within the enantiornithine radiation and Mesozoic birds as a whole.

Systematic palaeontology

Theropoda Marsh, 1881

Paraves Sereno, 1997

Avialae Gauthier, 1986

Ornithothoraces Chiappe, 1995

Enantiornithes Walker, 1981

Falcatakely forsterae gen. et sp. nov.

Etymology. "*Falcata*" (from Latin *falcatus*), meaning armed with a scythe, in reference to shape of rostrum; "*kely*" (Malagasy), meaning small; "forsterae," in recognition of Catherine A. Forster's contributions to work on Madagascan paravians.

Holotype. Partial cranium (University of Antananarivo [UA] 10015) consisting of rostrum, palate, and periorbital regions (Fig. 1, Extended Data Figs. 1 & 2, Supplemental Videos 1–8).

Locality and horizon. Locality MAD05-42, Berivotra Study Area, Upper Cretaceous (Maastrichtian; 72.1–66 Myr ago) Anembalemba Member, Maevarano Formation, Mahajanga Basin, northwestern Madagascar[22].

Diagnosis. Differs from other paravians based on the following combination of features (*indicates autapomorphies): extended, high maxilla that forms dorsal contour of rostrum*; dimpled texture on nasal and lacrimal, particularly on triangular caudodorsal process of latter*; lacrimal with caudally expanded ventral process*; large, flat jugal process of postorbital*. Further differs from most avialans by: long, straight quadratojugal process of jugal; antorbital fenestra nearly as long as tall. Further differs from other enantiornithines by: premaxilla slots into extended V-shaped sulcus of maxilla*; narrow rostrum (width at premaxilla-maxilla junction estimated at ~15% maximum width at rostral margin of orbit); nasal with distinct fossa near rostral end*.

Remarks. Avialae and Neornithes are used herein to delimit increasingly less inclusive monophyletic assemblages of theropod dinosaurs. Avialae (= "birds") refers to all theropods closer to living birds than to dromaeosaurids and troodontids (i.e., a stem-based monophyletic group containing *Passer domesticus* and all theropods closer to it than to *Dromaeosaurus* or *Troodon*). Neornithes represents the crown group of birds and is the equivalent of Aves (sensu ref. [23]); see Supplementary Information for additional phylogenetic definitions.

Cranial Osteology

UA 10015 pertains to an enantiornithine bird (estimated cranial length = 8.5 cm) with a high, but extremely narrow, preorbital region (Fig. 1). The lightly built face consists of a long, high edentulous maxilla and a short, tooth-bearing premaxilla, forming a rostrum unlike that of any known bird. The external nares are rostrally positioned and widely separated from a large, parallelogram-shaped antorbital fenestra. The premaxillae are fused rostrally and exhibit a short frontal process as in some other enantiornithines[5,24,25]. The maxillary process is short and slots into a V-shaped concavity on the maxilla (Fig. 1b, c; Extended Data Figs. 1f, 2c). A single, conical, unserrated tooth is preserved in the left premaxilla; the presence of additional premaxillary teeth is uncertain due to incomplete preservation.

The maxilla (<1 mm thick) of *Falcatakely* is unique among avialans in being extremely high and long, and forming at least 90% of the reconstructed pre-orbital rostrum height (Fig. 1c). It is unfenestrated, a condition shared with Enantiornithes (Supplementary Information), and lacks an antorbital fossa; it also preserves detailed vascular sulci over its surface indicating the presence of an expansive keratinous rhamphotheca (beak) in life[26] (Fig. 1a, Supplemental 3D PDF S1). The premaxillary process is well developed and forms part of the ventral border of the

external naris. An elongate, tapering caudoventral projection contributes to the jugal bar, delimiting the ventral border of the orbit where it underlies the lacrimal boot.

The elongate nasals expand in width caudally and are unique in possessing dorsomedially positioned fossae near the external nares (Extended Data Fig. 1b). The mid-portion of the nasals are broad and vaulted, as in bohaiornithid enantiornithines[5,27] and express surface dimpling on the lateral margin near the articulation with the lacrimal (Extended Data Fig. 1b–d). μCT-mediated reconstruction of *Falcatakely* reveals a nearly complete right lacrimal (Fig. 1c, Supplemental 3D PDF S2). The dorsal half of the element is T-shaped, as in avialans such as *Archaeopteryx*, *Pengornis*, and *Parapengornis*[2,27]. The rostrodorsal process is considerably longer than the caudodorsal process and is most similar to the condition in pengornithid enantiornithines (e.g., *Parapengornis*)[10]. The caudodorsal process is unique among avialans in morphology, being sub-triangular in shape, dimpled, and pneumatic (Extended Data Fig. 1d). The ventral ramus is longer than either the caudodorsal or rostrodorsal process, and is extensively excavated, as in pengornithids and bohaiornithids[2,19,27]. The ventral ramus terminates as a caudally expanded boot that sits just dorsal to the overlapping portions of the jugal and maxilla (Fig. 1c).

The jugal is triradiate with a long, dorsoventrally restricted maxillary process, a distinct postorbital process, and an extended, bar-like quadratojugal process (Extended Data Fig. 1e). In contrast to most avialans[21,28], the quadratojugal process is long and directed straight caudally, forming the ventral border of the infratemporal fenestra. The quadratojugal process is not bifurcated as in most non-avialan theropods and some phylogenetically early-branching birds like *Sapeornis*[29]. The right postorbital (Extended Data Fig. 1e) is represented only by its ventral process, which is flat and tapering, and quite unlike any known amongst avialans, or paravians

generally[30]. At least 15 scleral ossicles are present, enough to estimate the external diameter of the scleral ring at 16–18 mm (Fig. 1c).

The digitally reconstructed palate of UA 10015 (Extended Data Fig. 2) reveals a substantial level of detail not typically observable in Mesozoic avialans. The palatine is triradiate, with a long, thin rostral process that abuts the maxilla (Extended Data Fig. 2a). The palatine does not contact the jugal and only modestly contacts the pterygoid, but shares an elongate contact with the ectopterygoid. A dorsomedially directed choanal process sweeps toward the midline to join its antimere. UA 10015 preserves only the thin rostral processes of the pterygoids; these are in close association with the palatines (Extended Data Fig. 2a). The ectopterygoid, an element that is unknown in most Cretaceous avialans[24,31], is represented by a robust body and a thin, elongate, uncinate process that contacts the jugal bar (Extended Data Fig. 2a). The vomers are represented by two thin, dorsoventrally restricted laminar plates that extend rostrally between the two maxillae (Extended Data Fig. 2a, c). Thin sheets of bone are present just rostral to the pterygoids, potentially representing the expanded caudal end of the vomer, reminiscent of the condition in *Gobipteryx*[24,31].

Mosaic Evolution in the Avian Beak

Our phylogenetic analyses recover *Falcatakely* nested within Enantiornithes (Fig. 2, Extended Data Figs. 3, 4). The long, deep, and narrow rostrum of *Falcatakely*, dominated by an expanded maxilla, stands in stark contrast to the premaxilla+maxilla-formed facial region of other enantiornithines and more crownward non-neornithines. Even among rostrally elongated ornithothoracine taxa such as *Longipteryx*, *Longirostravis*, and *Dingavis*, this morphology is

155 achieved through concomitant reduction in premaxillary and maxillary height as bones elongate
156 along the rostrocaudal axis[5,6,12,14,15].

157 Quantitative assessment of non-avialan and avialan (including Neornithes) facial shape
158 demonstrates the unique combination in *Falcatakely* of a derived cranial phenotype (i.e., a
159 neornithine-like expanded rostrum) formed by an underlying plesiomorphic paravian skeletal
160 framework. We used 2D geometric morphometrics (Fig. 3) to compare maxillary and
161 premaxillary shape in UA 10015 with that of a sample of fossil non-avialan theropods, as well as
162 the crown birds *Gallus gallus* (red junglefowl) and *Nothoprocta pentlandii* (Andean tinamou).
163 Principal component analysis (PCA) reveals that species group together based on the ratio of
164 maxillary to premaxillary size (PC axis 1) and the ratio of rostrocaudal length to dorsoventral
165 height of both elements (PC axis 2). Despite having maxillary and premaxillary proportions
166 similar to those of non-avialan theropods (e.g., paravians, oviraptorosaurs, ornithomimosaurs),
167 *Falcatakely* exhibits an overall rostrum phenotype convergent upon a number of neornithine
168 groups.

169 The configuration of the individual skeletal elements in *Falcatakely* is more similar to the
170 non-avialans *Microraptor* and *Zanabazar* than to ornithuromorphs (including neornithines) due
171 to the expanded maxilla and relatively small premaxilla. Nonetheless, the three-dimensional
172 shape of the pre-orbital facial skeleton closely resembles that of some extant birds (Extended
173 Data Figs. 5, 6), as assessed using 3D geometric morphometrics to compare the shape of the
174 maxilla, premaxilla, and nasal within a sample of 349 extant birds (Supplementary
175 Information)[32]. PCA of rostrum shape reveals that *Falcatakely* occupies a position in whole-
176 rostrum morphospace that is quantitatively similar to those of a number of unrelated
177 neornithines, including members of Ramphastidae (toucans), Phaethonidae (tropicbirds),

178 Columbidae (pigeons and doves), and Tyrannidae (tyrant flycatchers) (see interactive 3D plot
179 associated with online materials).

180 The discovery of *Falcatakely* expands the realized cranial morphology among known
181 non-neornithine birds considerably. Analysis of its three-dimensional anatomy reveals a stem
182 bird occupying a previously unrealized position in rostrum morphospace and potentially
183 exploiting an ecology not again seen until the diversification of crown-group birds in the mid-
184 Cenozoic. A partial emancipation of the palate from the facial skeleton (i.e., loss of jugal contact
185 with the palatine) concurrent with heretofore unappreciated rostrum elaboration suggests that
186 these regions are functionally and developmentally integrated[16,31,33]. Interestingly, a mosaic
187 pattern of palatal release is exhibited among stem avialans, at least insofar as the functional
188 demands of the rostrum/beak in *Falcatakely* appears to have required reinforcement of the
189 connections to the rear of the face. These connections are maintained through both the
190 ectopterygoid and with retention of the robust postorbital linkage, despite the loss of the mid-
191 face palatine connection to the jugal bar. Such an arrangement was likely necessary for
192 stabilizing the mid-portion of the cranium and the long, high, and extremely narrow rostrum.
193 Although incomplete, the presence of a robust postorbital further indicates a rigidly enforced
194 caudal region of the cranium[7].

195 The maxilla-dominated facial skeleton of *Falcatakely* reveals two important insights for
196 the evolutionary history of birds. First, the ancestral developmental patterning of rostrum
197 construction in basal avialans has generated neornithine-like cranial phenotypes not recognized
198 in the fossil record until now. Second, the developmental reduction of the maxilla previously
199 inferred for Ornithothoraces[7,9] was not a fixed trait, at least among enantiornithine birds. Thus,
200 consolidation to a premaxilla-dominated rostrum, a hallmark of all living birds, was not an

evolutionary prerequisite for rostrum, and thus, beak enlargement. More generally, this is consistent with a growing appreciation for the flexibility of underlying developmental mechanisms[8,34,35] that may be responsible for generating convergent morphology among distantly related forms. With *Falcatakely*, this appreciation can now be extended to the deep time avialan record. The discovery of *Falcatakely* expands the ecomorphological potential realized by enantiornithines and Mesozoic birds more generally[3,18]. This new appreciation of avialan anatomy underscores the potential for significant variability in trophic ecology during the first great diversification of the group during the Cretaceous Period[5,6,36,37].

Online Content

Detailed methods, along with additional Extended Data display items, Source Data, Nature Research reporting summary, details of authors contributions and competing interests statement, etc. are available in the online version of the paper at https://XXXX XXXX XXXX; references unique to these sections appear only in the online paper. Additional supporting information (e.g., interactive PDFs; matrices and executable files) are available on DRYAD at: https://doi.org/10.5061/dryad.mkkwh70wg.

1. Xu, X. et al. An integrative approach to understanding bird origins. *Science* **346**, 1–10 (2014).
2. Zhou, Z., Clarke, J. & Zhang, F. Insight into diversity, body size and morphological evolution from the largest Early Cretaceous enantiornithine bird. *J. Anat.* **212**, 565–577 (2008).

3. Brusatte, S. L., O'Connor, J. K. & Jarvis, E. D. The origin and diversification of birds. *Curr. Biol.* **25**, R888–R898 (2015).

4. O'Connor, J. K. in *The Evolution of Feathers* (eds Foth, C. & Rauhut, O. W. M.) 147–172 (Springer, 2020).

5. O'Connor, J. K. & Chiappe, L. M. A revision of enantiornithine (Aves: Ornithothoraces) skull morphology. *J. Syst. Palaeontol.* **9**, 135–157 (2011).

6. Huang, J. et al. A new ornithurine from the Early Cretaceous of China sheds light on the evolution of early ecological and cranial diversity in birds. *PeerJ* **4**, e1765 (2016).

7. Bhullar, B.-A. S. et al. How to make a bird skull: major transitions in the evolution of the avian cranium, paedomorphosis, and the beak as a surrogate hand. *Integr. Comp. Biol*. **56**, 389–403 (2016).

8. Young, N. M. et al. Embryonic bauplans and the developmental origins of facial diversity and constraint. *Development* **141**, 1059–1063 (2014).

9. Mayr, G. Comparative morphology of the avian maxillary bone (os maxillare) based on an examination of macerated juvenile skeletons. *Acta Zool.* **101**, 24–38 (2020).

10. Hu, H., O'Connor, J. K. & Zhou, Z. A new species of Pengornithidae (Aves: Enantiornithes) from the Lower Cretaceous of China suggests a specialized scansorial habitat previously unknown in early birds. *PLoS ONE* **10**, e0126791 (2015).

11. Bailleul, A. M. et al. An Early Cretaceous enantiornithine (Aves) preserving an unlaid egg and probable medullary bone. *Nature Comm.* **10**, 1275 (2019).

12. Hou, L., Chiappe, L. M., Zhang, F. & Chuong, C.-M. New Early Cretaceous fossil from China documents a novel trophic specialization for Mesozoic birds. *Naturwissenschaften* **91**, 22–25 (2004).

13. O'Connor, J. K. et al. Phylogenetic support for a specialized clade of Cretaceous enantiornithine birds with information from a new species. *J. Vertebr. Paleontol.* **29**, 188–204 (2009).
14. O'Connor, J. K., Chiappe, L. M., Gao, C. & Zhao, B. Anatomy of the Early Cretaceous enantiornithine bird *Rapaxavis pani*. *Acta Palaeontol. Pol.* **56**, 463–475 (2011).
15. O'Connor, J. K., Wang, M. & Hu, H. A new ornithuromorph (Aves) with an elongate rostrum from the Jehol Biota, and the early evolution of rostralization in birds. *J. Syst. Palaeontol.* **14**, 939–948 (2016).
16. Field, D. J. et al. Complete *Ichthyornis* skull illuminates mosaic assembly of the avian head. *Nature* **557**, 96–100 (2018).
17. Field, D. J., Benito, J., Chen, A., Jagt, J. W. M. & Ksepka, D. T. Late Cretaceous neornithine from Europe illuminates the origins of crown birds. *Nature* **579**, 397–401 (2020).
18. Chiappe, L. M. & Witmer, L. M. *Mesozoic Birds: Above the Heads of Dinosaurs* (Univ. California Press, 2004).
19. Li, Z., Zhou, Z., Wang, M. & Clarke, J. A. A new specimen of large-bodied basal enantiornithine *Bohaiornis* from the Early Cretaceous of China and the inference of feeding ecology in Mesozoic birds. *J. Paleontol.* **88**, 99–108 (2014).
20. Wang, M., Hu, H. & Li, Z. A new small enantiornithine bird from the Jehol Biota, with implications for early evolution of avian skull morphology. *J. Syst. Palaeontol.* **14**, 481–497 (2016).
21. Wang, M., O'Connor, J. K. & Zhou, Z. A new robust enantiornithine bird from the Lower Cretaceous of China with scansorial adaptations. *J. Vertebr. Paleontol.* **34**, 657–671 (2014).

22. Rogers, R. R., Hartman, J. H. & Krause, D. W. Stratigraphic analysis of Upper Cretaceous rocks in the Mahajanga Basin, northwestern Madagascar: implications for ancient and modern faunas. *J. Geol.* **108**, 275–301 (2000).
23. Gauthier, J.A., & de Queiroz, K. in *New Perspectives on the Origin and Early Evolution of Birds: Proceedings of the International Symposium in Honor of John H. Ostrom* (eds Gauthier, J. & Gall, L. F.). 7–41 (Peabody Museum of Natural History, Yale University, 2001).
24. Chiappe, L. M., Norell, M. A. & Clark, J. M. A new skull of *Gobipteryx minuta* (Aves: Enantiornithes) from the Cretaceous of the Gobi Desert. *Amer. Mus. Novitates* **3364**, 1–15 (2001).
25. Wang, M. & Zhou, Z. A new enantiornithine (Aves: Ornithothoraces) with completely fused premaxillae from the Early Cretaceous of China. *J. Syst. Palaeontol.* **17**, 1299–1312 (2019).
26. Hieronymus, T. L. & Witmer, L. M. Homology and evolution of avian compound rhamphothecae. *Auk* **127**, 590–604 (2010).
27. Wang, M., Zhou, Z.-H., O'Connor, J. K. & Zelenkov, N. V. A new diverse enantiornithine family (Bohaiornithidae fam. nov.) from the Lower Cretaceous of China with information from two new species. *Vert. Palasiat.* **52**, 31–76 (2014).
28. Wang, M. & Hu, H. A comparative morphological study of the jugal and quadratojugal in early birds and their dinosaurian relatives. *Anat. Rec.* **300**, 62–75 (2017).
29. Wang, Y. et al. A previously undescribed specimen reveals new information on the dentition of *Sapeornis chaoyangensis*. *Cret. Res.* **74**, 1–10 (2017).

30. Hu, H., O'Connor, J. K., Wang, M., Wroe, S. & McDonald, P. G. New anatomical information on the bohaiornithid *Longusunguis* and the presence of a plesiomorphic diapsid skull in Enantiornithes. *J. Syst. Palaeontol.* **18**, 1481–1495 (2020).
31. Hu, H. et al. Evolution of the vomer and its implications for cranial kinesis in Paraves. *Proc. Natl. Acad. Sci. USA* **116,** 19571–19578 (2019).
32. Felice, R. N. & Goswami, A. Developmental origins of mosaic evolution in the avian cranium. *Proc. Natl. Acad. Sci. USA* **115**, 555–560 (2018).
33. Bhullar, B.-A. S. et al. A molecular mechanism for the origin of a key evolutionary innovation, the bird beak and palate, revealed by an integrative approach to major transitions in vertebrate history. *Evolution* **69**, 1665–1677 (2015).
34. Mallarino, R. et al. Closely related bird species demonstrate flexibility between beak morphology and underlying developmental programs. *Proc. Natl. Acad. Sci. USA* **109**, 16222–16227 (2012).
35. Tokita, M., Yano, W., James, H. F. & Abzhanov, A. Cranial shape evolution in adaptive radiations of birds: comparative morphometrics of Darwin's finches and Hawaiian honeycreepers. *Phil. Trans. R. Soc. B* **372**, 20150481 (2016).
36. Bell, A. & Chiappe, L. M. Statistical approaches for inferring ecology in Mesozoic birds. *J. Syst. Palaeontol.* **9**, 119–133 (2011).
37. O'Connor, J. K. The trophic habits of early birds. *Palaeogeog. Palaeoclim. Palaeoecol.* **513**, 178–195 (2019).

MAIN FIGURE LEGENDS:

Fig. 1 | Cranium of the Cretaceous enantiornithine bird *Falcatakely forsterae* (UA 10015, holotype). a, Photograph of specimen, with right lateral view of pre-orbital region (right side of image) and ventral view of palatal region (left side of image); **b**, Digital polygon reconstruction from μCT scan of specimen in **a**; **c**, Digital polygon reconstruction of specimen with most elements in **b** placed in near-life position in right lateral view; **d**, Line drawing reconstruction (not to scale) illustrating preserved (in white) elements of cranium. Left and right sides indicated as (l) and (r), respectively. AOF, antorbital fenestra; ect, ectopterygoid; EN, external nares; ITF, infratemporal fenestra; jpmx, jugal process of maxilla; ju, jugal; lc, lacrimal; mpmx, midline premaxilla; mx, maxilla; na, nasal; pal, palatine; pmx, premaxilla; po, postorbital; pter, pterygoid; qj, quadratojugal; sr, scleral ring; to, tooth. [Planned for column width (89 mm); colour]

Fig. 2 | Mosaic evolution of the avialan facial skeleton as depicted among selected early-branching forms. Phylogenetic analysis places *Falcatakely forsterae* among enantiornithine birds. Illustration for *Xinghaiornis*(*) placed near its approximate position in the phylogeny and based on ref. [15]. Illustrations not to scale. Colour coding: premaxilla, red; maxilla, green; nasal, yellow; lacrimal, lavender; dentary, blue. Images for *Archaeopteryx*, *Ichthyornis*, *Hesperornis*, and *Gallus* modified from ref. [16] (see Supplementary Information for additional details for included taxa and phylogenetic analyses). [Planned for 1 ½ column width (136 mm); colour]

Fig. 3 | Geometric morphometric analyses of facial shape in *Falcatakely forsterae* among paravians. Plot of first two principal components of 2D landmark analysis of maxillary (blue

line segments) and premaxillary (red line segments) morphology of select theropod taxa. Unique configuration of maxilla and premaxilla in *Falcatakely* is more similar to that of non-avialans in a two-dimensional analysis focused on fossil taxa, although overall three-dimensional rostrum phenotype occupies morphospace converged upon by subsequent radiations of neornithine birds (hyperlink to HTML file). See Supplementary Information for analytical protocols. [Planned for column width (89 mm); colour]

EXTENDED DATA FIGURES

Extended Data Fig. 1 | Rostrum of the Cretaceous enantiornithine bird *Falcatakely forsterae* (UA 10015, holotype). a, Line drawing reconstruction (not to scale) illustrating preserved (in white) elements of cranium; **b**, Digital polygon surface reconstruction (from µCT scans) of right nasal in rostrodorsal view (caudal to top) highlighting midline depression and dimpled surface texture; **c**, Digital polygon surface reconstruction of right nasal in dorsal view illustrating dimpled architecture on frontal and rostral portions, which extends laterally onto lacrimal; **d**, Digital polygon surface reconstruction of right facial elements in right lateral view to illustrate shape and inter-element relationships of nasal, maxilla, and lacrimal (note surface texture of right maxilla with neurovascular sulci broadly expressed over lateral surface, deep to inferred keratinous covering (i.e., beak)); **e,** Digital polygon surface reconstruction of lower lateral face to highlight arrangement of maxilla, lacrimal, jugal, and postorbital (all elements from right side); **f,** Digital polygon surface reconstruction of left maxilla and premaxilla articulation (rostral to left). AOF, antorbital fenestra; cdp, caudodorsal process of lacrimal; cp, choanal process of palatine; ect, ectopterygoid; EN, external nares; ITF, infratemporal fenestra; fpn, frontal process of nasal; inb, internarial bar; jpmx, jugal process of maxilla; ju, jugal; lbo,

lacrimal boot; lc, lacrimal; ld, lacrimal dimpling; le, lacrimal excavation; lf, lacrimal foramen; mpmx, midline premaxilla; mx, maxilla; mxpj, maxillary process of jugal; na, nasal; nd, nasal dimpling; nf, nasal fossa; nvs, neurovascular sulci; pal, palatine; pmpm, premaxillary process of maxilla; pmx, premaxilla; po, postorbital; qj, quadratojugal; rdp, rostrodorsal process of lacrimal; rpn, rostral process of nasal; tm, tomial margin; to, tooth; vr, ventral ramus of lacrimal. [Planned for page width; greyscale]

Extended Data Fig. 2 | Palatal and lateral facial regions of the Cretaceous enantiornithine bird *Falcatakely forsterae* (UA 10015, holotype). **a**, Digital polygon surface reconstruction (from µCT scans) of palate and lateral face in ventral view; **b**, Reconstructed outline drawing of *Falcatakely* in palatal view (shaded regions not preserved); **c**, Digital polygon surface reconstruction of internal aspect of left facial skeleton (premaxilla, maxilla, nasal) and palate in right lateral view. Left and right sides indicated as (l) and (r), respectively. Dashed line in **c** represents approximate contour of caudal margin (i.e., ventral ramus of lacrimal) of antorbital fenestra. Scale bar in image serves for both 2a and 2c; reconstruction in 2b not to same scale. AOF, antorbital fenestra; bs, basisphenoid rostrum; cp, choanal process of (right) palatine; ect, ectopterygoid; EN, external nares; jpmx, jugal process of maxilla; mpmx, midline premaxilla; mx, maxilla; na, nasal; pal, palatine; pmx, premaxilla; pter, pterygoid; to, tooth; up, uncinate process of ectopterygoid; vm, vomers. [Planned for 2/3 page width; colour]

Extended Data Fig. 3 | Majority rule tree of *Falcatakely* among coelurosaurians from Bayesian analysis of the Theropod Working Group matrix (TWiG). Clades outside of

Avialae are collapsed for brevity. Posterior probabilities are placed above nodes. [Planned for page width; colour]

Extended Data Fig. 4 | Majority rule tree of *Falcatakely* among avialans from Bayesian analysis of modified Wang and Zhou (2019) matrix. Posterior probabilities are placed above nodes. [Planned for page width; colour]

Extended Data Figure 5 | Geometric morphometric analysis of rostrum shape in *Falcatakely forsterae* among avians. Plot of first two principal components of 3D landmark analysis of total rostrum shape of *Falcatakely* and extant avian taxa. Whereas unique configuration of maxilla and premaxilla in *Falcatakely* is more similar to those of non-avialan paravians (Fig. 3), overall three-dimensional rostrum phenotype occupies morphospace converged upon by subsequent radiations of neornithine birds (hyperlink to HTML file). See Supplementary Information for analytical protocols. [Planned for column width (89 mm); colour]

Extended Data Figure 6 | Landmarking procedure for 3D geometric morphometric analysis in dorsal (a) and lateral (b) views. Red points represent anatomical (Type I) landmarks, yellow points are sliding semi-landmarks. [Planned for 2/3 page width; colour]

Supplemental Data File: Interactive morphospace plot of 3D rostrum shape. Plot of first two principal components of 3D landmark analysis of rostrum of *Falcatakely forsterae* and extant

400 avian taxa. Hovering over data points reveals species name and order. Supraordinal groups can
401 be toggled on/off by clicking on legend.

402

403 METHODS

404 **Temporal and Stratigraphic context.** UA 10015 was recovered in 2010 at locality MAD05-42
405 in the Berivotra Study Area of the Mahajanga Basin Project. The bone-bearing horizon lies
406 within Facies 2 of the Anembalemba Member in the Upper Cretaceous (Maastrichtian)
407 Maevarano Formation[22] (Supplementary Information). Many specimens, including UA 10015,
408 recovered from the Anembalemba Member were entombed as part of rapid debris flows, often
409 resulting in spectacular preservation with only minimal displacement and taphonomic distortion
410 during burial[38,39].

411 **Phylogenetic methods.** Given the extremely derived condition in *Falcatakely* and the notable
412 amount of homoplasy among non-avialan paravians and basal avialans, we employed a two-
413 tiered dataset approach in an effort to best constrain the phylogenetic affinities of *Falcatakely*
414 (Supplementary Information). First, we utilized the densely sampled, coelurosaur-wide Theropod
415 Working Group matrix (TWiG)[40,41] to broadly assess and confirm the position of *Falcatakely*
416 among paravians (Extended Data Fig. 3, Supplementary Information). Next, we employed a
417 modified version of a well-established Mesozoic avialan-focused matrix (WEA[25]), along with
418 modifications from ref. [16], to further examine the relationship of *Falcatakely* among avialans
419 (Fig. 2, Extended Data Fig. 4). Bayesian inference (BI) trees were estimated for each dataset
420 using MrBayes v3.2[42]. The standard model (Markov *k*-state variable model [Mkv][43]) was
421 specified with gamma-distributed rate variation (see ref. [44]). A subset of characters was set as
422 ordered, following the prior usage of the included datasets. During the analysis, Markov Chain

Monte Carlo (MCMC) convergence was assessed using the average standard deviation of split frequencies and examining the trace files in Tracer[45]. Convergence to stationarity was assumed for split frequencies below 0.01 and effective sample size (ESS) values >200. All analyses were performed with two runs of four chains each, run for 10 million generations, sampling parameters every 1000 generations. The first 25% of samples were discarded as burn-in. Results are summarized using a majority rule consensus (MRC) tree[46]. MRC trees for both datasets depict *Falcatakely* as a member of Enantiornithes. The TWiG dataset set recovers it as the sister taxon to *Pengornis*, whereas the WEA matrix finds it in a large polytomy with other enantiornithines (Extended Data Figs. 3, 4). Given the denser avialan sampling in the WEA dataset, the phylogenetic results from this matrix are used here as the primary results. Clade support was assessed using the estimated posterior probabilities from the BI trees. Morphological character support was established for MRC trees using the *map* and *apo* commands in TNT[47–49.] Additional details of phylogenetic results and clade support are presented in the Supplementary Information.

To further interrogate the robustness of our inferred trees, three sensitivity analyses were run examining the influence of cranial vs. postcranial data and the potential impact of cranial data-only taxa on tree inference. These analyses reveal no significant topological alterations relative to the standard analysis detailed above, lending support to the primary results placing *Falcatakely* among enantiornithine birds. Moreover, additional explicit hypothesis testing via Bayes Factors comparisons was conducted with *Falcatakely* constrained to stemward positions (e.g., with *Falcatakely* excluded from Pygostylia), which resulted in suboptimal solutions. Details for these analyses and the specifics of the results are provided in the Supplementary

Information, with executable files for the sensitivity and alternative hypothesis testing available on DRYAD at: https://doi.org/10.5061/dryad.mkkwh70wg.

References specific to online-only materials

38. Rogers, R. R. Fine-grained debris flows and extraordinary vertebrate burials in the Late Cretaceous of Madagascar. *Geology* **33**, 297–300 (2005).
39. Rogers, R. R., Krause, D. W., Curry Rogers, K., Rasoamiaramanana, A. H. & Rahantarisoa, L. Paleoenvironment and paleoecology of *Majungasaurus crenatissimus* (Theropoda: Abelisauridae) from the Late Cretaceous of Madagascar. *J. Vertebr. Paleontol.* **27,** suppl. to Issue 2, 21–31 (2007).
40. Brusatte, S. L., Lloyd, G. T., Wang, S. C. & Norell, M. A. Gradual assembly of avian body plan culminated in rapid rates of evolution across dinosaur-bird transition. *Curr. Biol.* **24**, 2386–2392 (2014).
41. Turner, A. H., Makovicky, P. J. & Norell, M. A. A review of dromaeosaurid systematics and paravian phylogeny. *Bull. Amer. Mus. Nat. Hist.* **371**, 1–206 (2012).
42. Ronquist, F. et al. MrBayes 3.2: efficient Bayesian phylogenetic inference and model choice across a large model space. *Syst. Biol.* **61**, 539–542 (2012).
43. Lewis, P. O. A likelihood approach to estimating phylogeny from discrete morphological character data. *Syst. Biol.* **50**, 913–925 (2001).
44. Clarke, J. A. & Middleton, K. M. Mosaicism, modules, and the evolution of birds: results from a Bayesian approach to the study of morphological evolution using discrete character data. *Syst. Biol.* **57**, 185–201 (2008).

45. Rambaut A., Suchard, M. A., Xie, D. & Drummond, A. J. Tracer v1.6, Available from http://beast.bio.ed.ac.uk/Tracer (2014).
46. O'Reilly, J. E. & Donoghue, P. C. J. The efficacy of consensus tree methods for summarizing phylogenetic relationships from a posterior sample of trees estimated from morphological data. *Syst. Biol.* **67**, 354–362 (2017).
47. Goloboff, P.A., Farris, J. & Nixon, K. TNT: a free program for phylogenetic analysis. *Cladistics* **24**, 774–786 (2008).
48. Goloboff, P.A., Farris, J. S., & Nixon, K. C. TNT: Tree Analysis Using New Technology, vers. 1.1 (Willi Hennig Society Edition). Program and documentation available at http://www.zmuc.dk/public/phylogeny.html (2008).
49. Goloboff, P. A. & Catalano, S. A. TNT version 1.5, including a full implementation of phylogenetic morphometrics. *Cladistics* **32**, 221–238 (2016).

Acknowledgements We thank the Université d'Antananarivo, the Mahajanga Basin Project field teams, and the villagers of the Berivotra Study Area for support; the ministries of Mines, Higher Education, and Culture of the Republic of Madagascar for permission to conduct field research; the National Geographic Society (8597-09) and the US National Science Foundation (EAR–0446488, EAR–1525915, EAR–1664432) for funding; and M. Witton for drafting line drawings used in Fig. 1 and Extended Data Figs. 1 & 2. Collection of avian 3D morphometric data was funded by European Research Council grant no. STG-2014-637171 (to A. Goswami). Full acknowledgments are provided in the Supplementary Information.

Author Contributions: P.M.O., A.H.T., and J.R.G. designed the project; P.M.O., A.H.T.,

J.R.G., R.R.R., D.W.K. and L.J.R. conducted the fieldwork. J.R.G. performed mechanical preparation of the specimen; J.R.G. and P.M.O. conducted μCT digital preparation/interpretation and rapid prototyping of UA 10015; R.R.R. and L.J.R. provided geological data and taphonomic interpretation; P.M.O., A.H.T., J.R.G., and R.N.F. completed lab work on the fossil and digital representation thereof and provided input on descriptions and comparisons; A.H.T. and P.M.O. contributed to the character coding and phylogenetic analysis; R.N.F. completed the morphometric analyses; P.M.O., A.H.T., and J.R.G. developed the manuscript, with contributions and/or editing from all authors.

Additional Information

Supplementary Information is available in the online version of the paper at http://XXXX XXXX.

Author Information Reprints and permissions information is available at www.nature.com/reprints. The authors declare no competing financial interests. Readers are welcome to comment on the online version of the paper. Publisher's note: Springer Nature remains neutral with regard to jurisdictional claims in published maps and institutional affiliations. Correspondence and requests for materials should be addressed to P.M.O. (oconnorp@ohio.edu).

Data Availability

512 UA 10015 is cataloged into the collections at the Université d'Antananarivo. Details regarding
513 digital file development and derivatives of files (e.g., DICOM, PLY) used as part of the study are
514 included in the Supplementary Information and archived on the MorphoSource website
515 (https://www.morphosource.org/Detail/ProjectDetail/Show/project_id/7894). Phylogenetic
516 character information and parameters used in the analyses are provided in the Supplementary
517 Information. Executable files for phylogenetic analyses, interactive 3D morphospace plot, and
518 interactive 3D PDFs are hosted on DRYAD: https://doi.org/10.5061/dryad.mkkwh70wg. This
519 published work, including the novel genus (urn:lsid:zoobank.org:act:5BA26059-B428-4896-
520 BFEA-2475419C61FC) and species (urn:lsid:zoobank.org:act:69314771-F0D8-4C15-946C-
521 524164385FB7) along with the associated nomenclatural acts, have been registered in ZooBank:
522 urn:lsid:zoobank.org:pub:4595D69E-FE12-4DAD-B155-89F084254F73.
523
524
525
526
527
528
529
530
531
532

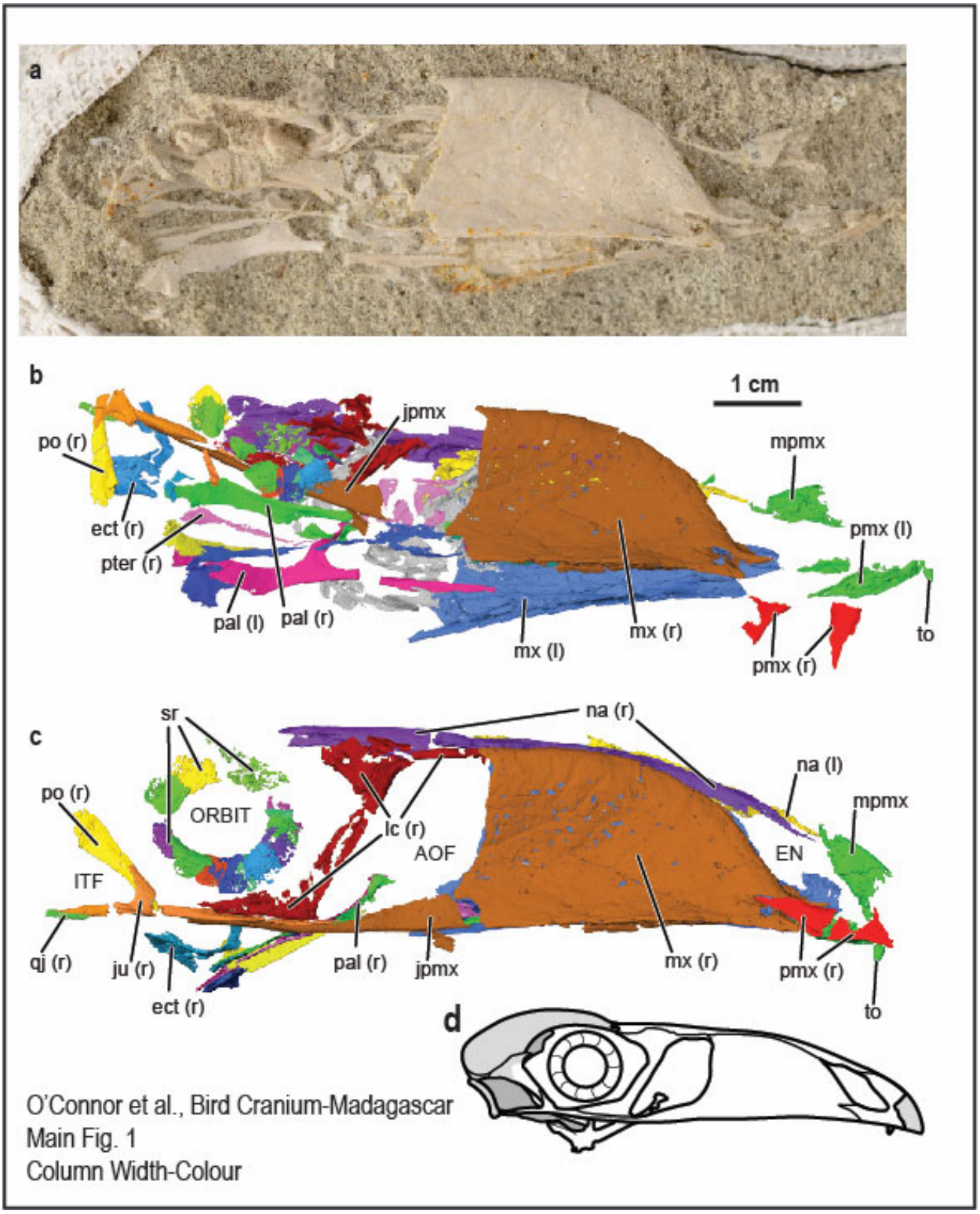
a
b
1 cm
po (r)
jpmx
mpmx
ect (r)
pmx (l)
pter (r)
pal (l)
pal (r)
mx (l)
mx (r)
pmx (r)
to
c
sr
na (r)
na (l)
po (r)
ORBIT
lc (r)
mpmx
AOF
EN
ITF
qj (r)
ju (r)
pal (r)
jpmx
mx (r)
pmx (r)
ect (r)
to
d
O'Connor et al., Bird Cranium-Madagascar
Main Fig. 1
Column Width-Colour

533

534

535

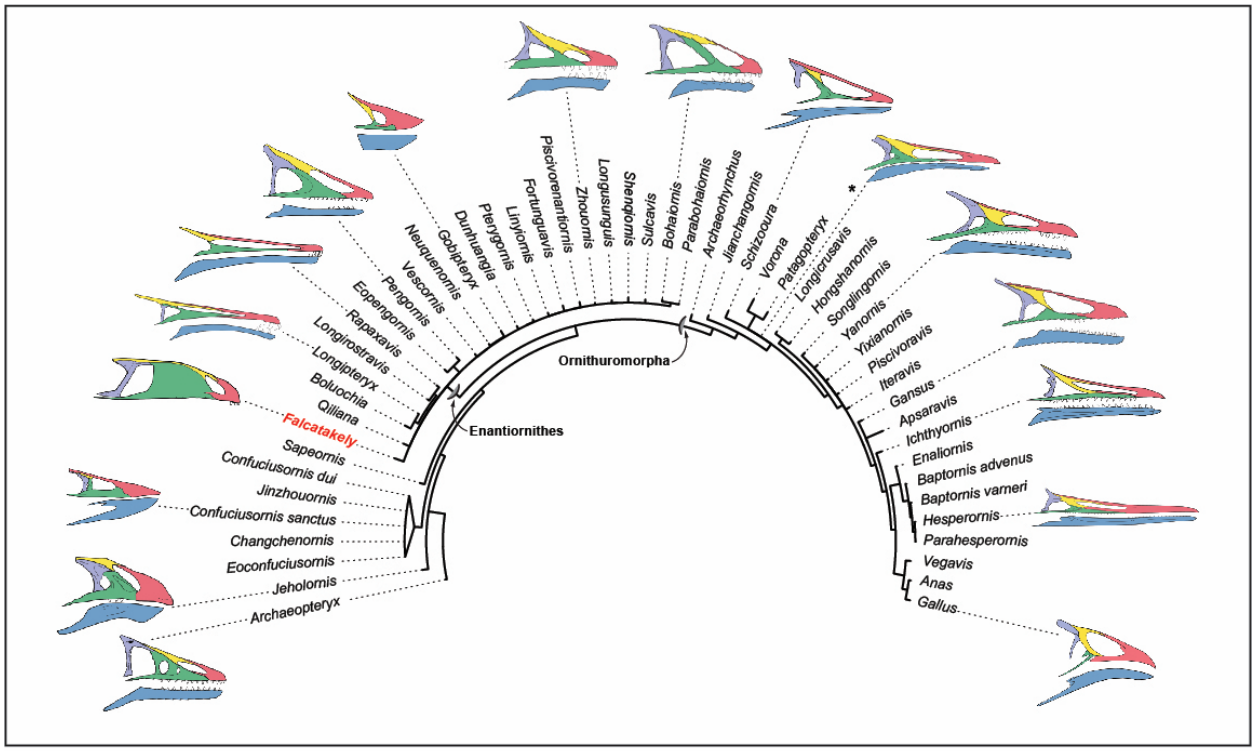

O'Connor et al., Bird Cranium-Madagascar
Main Fig. 2
1 1/2 Column Width-Colour

536

537

538

539

540

541

542

543

544

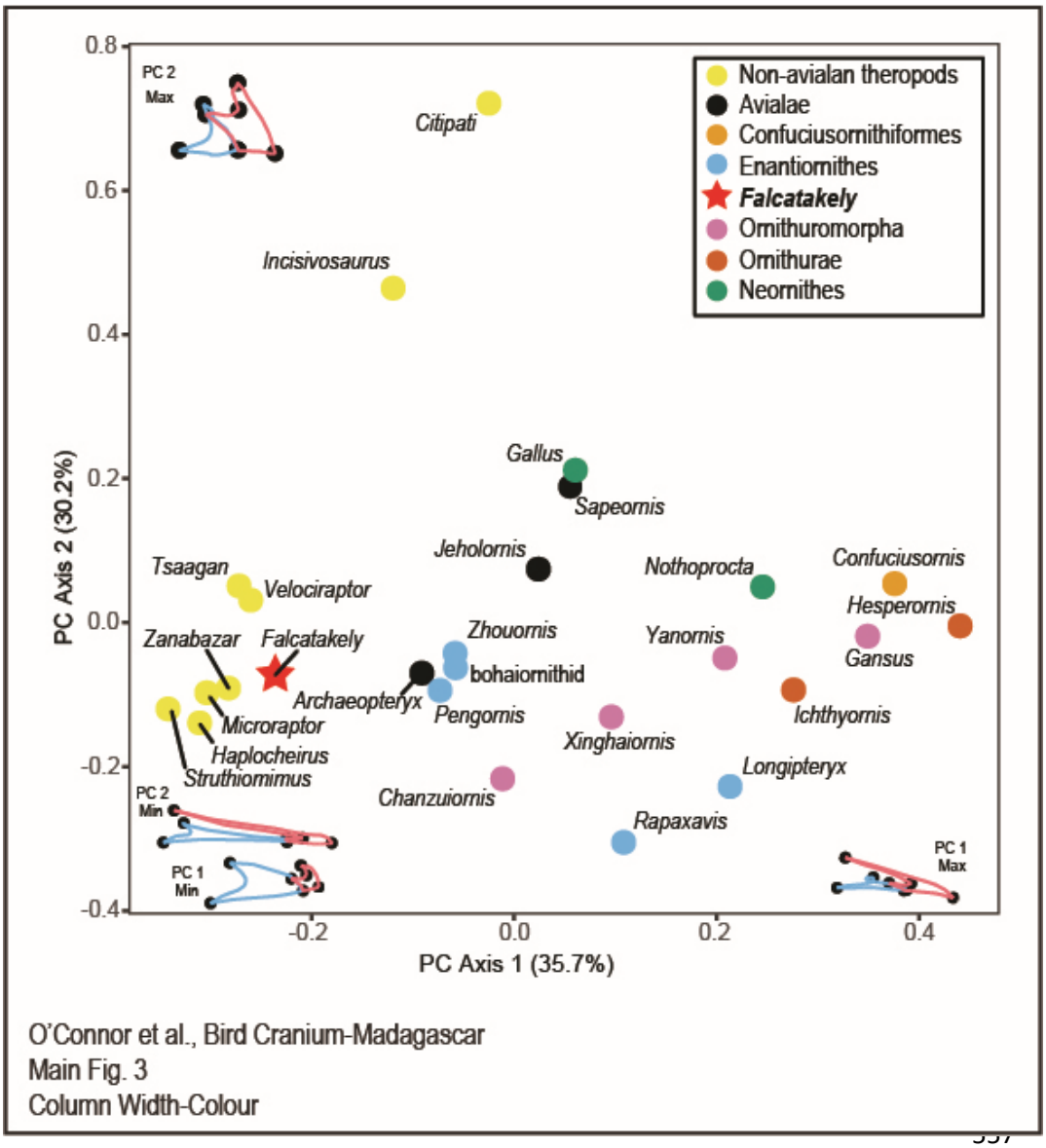

O'Connor et al., Bird Cranium-Madagascar
Main Fig. 3
Column Width-Colour

558

559

560

561

562

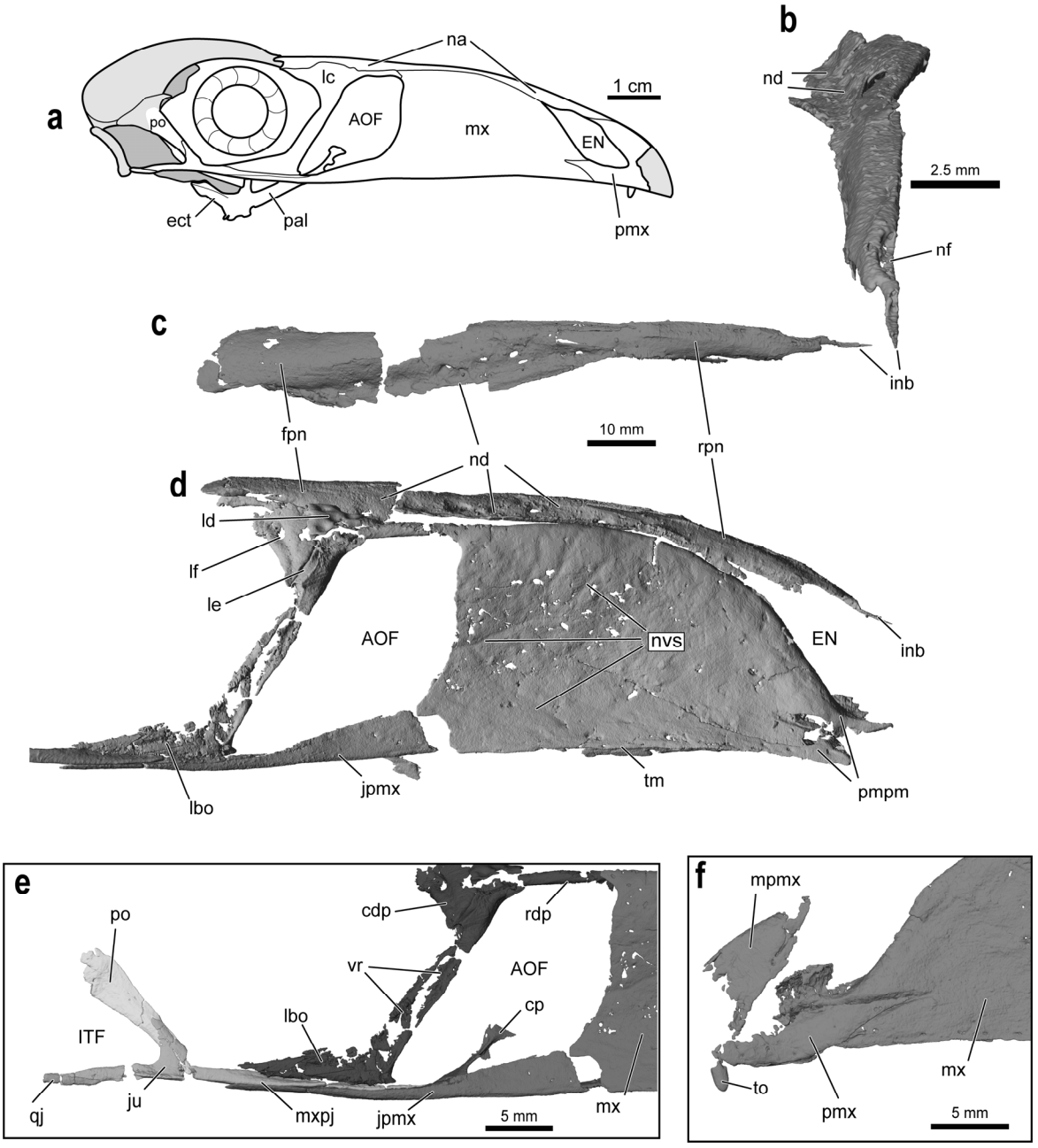

563

564 O'Connor et al. Extended Data Figure 1—Full-page width—greyscale.

565

566

567

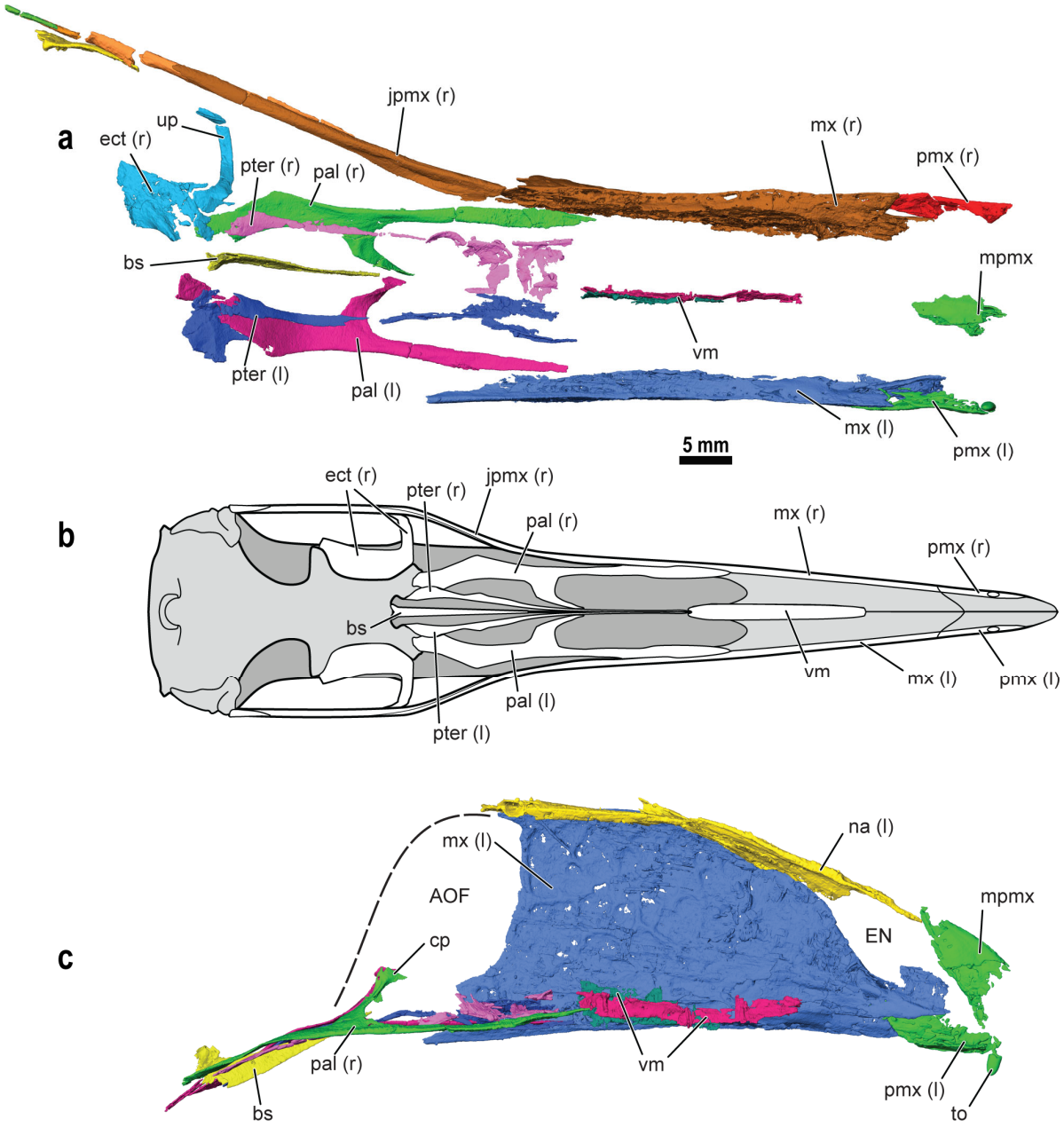

568

569 O'Connor et al. Extended Data Figure 2—Full-page width—Colour.

570

571

572

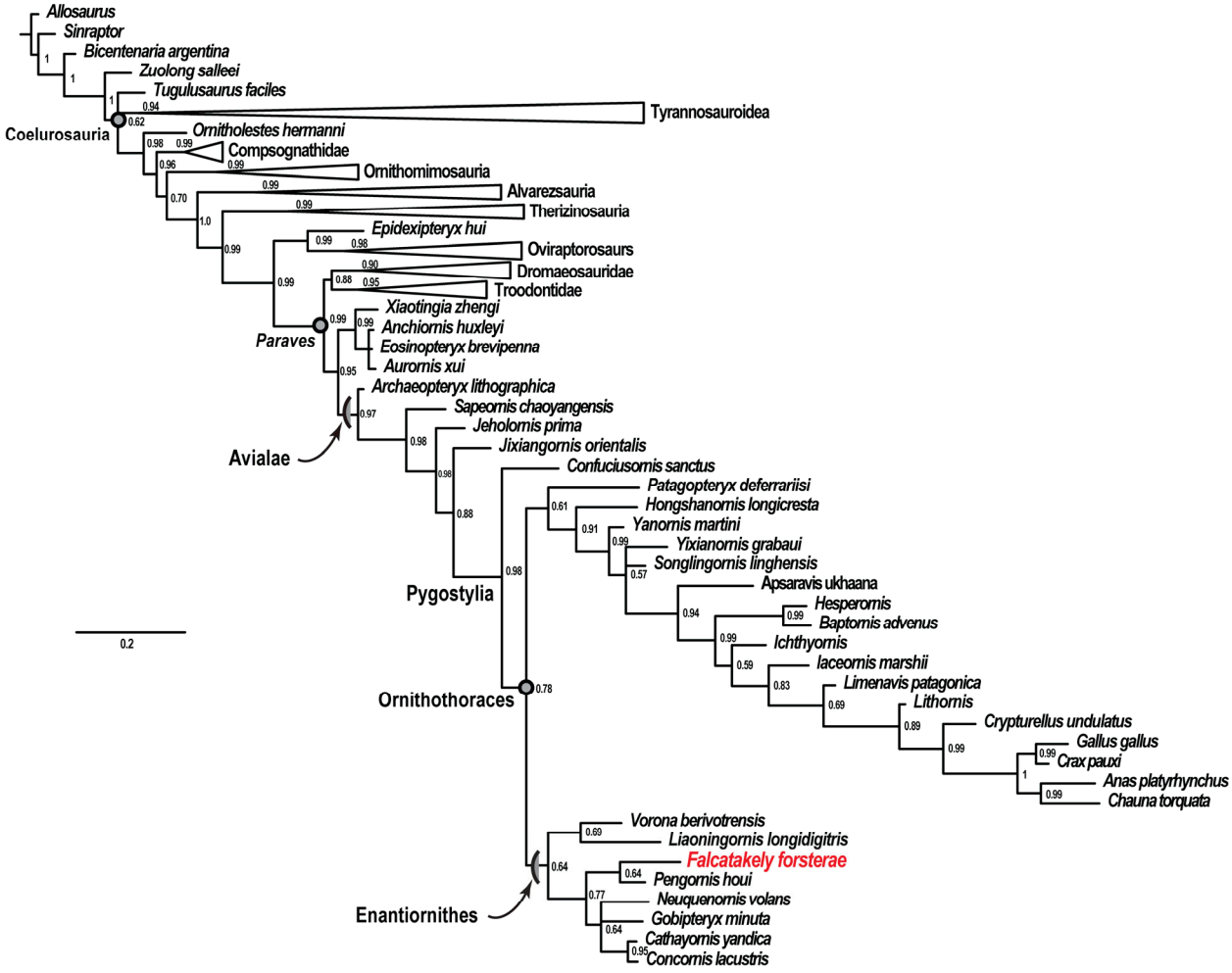

O’Connor et al. Extended Data Figure 3—Full-page width—Colour.

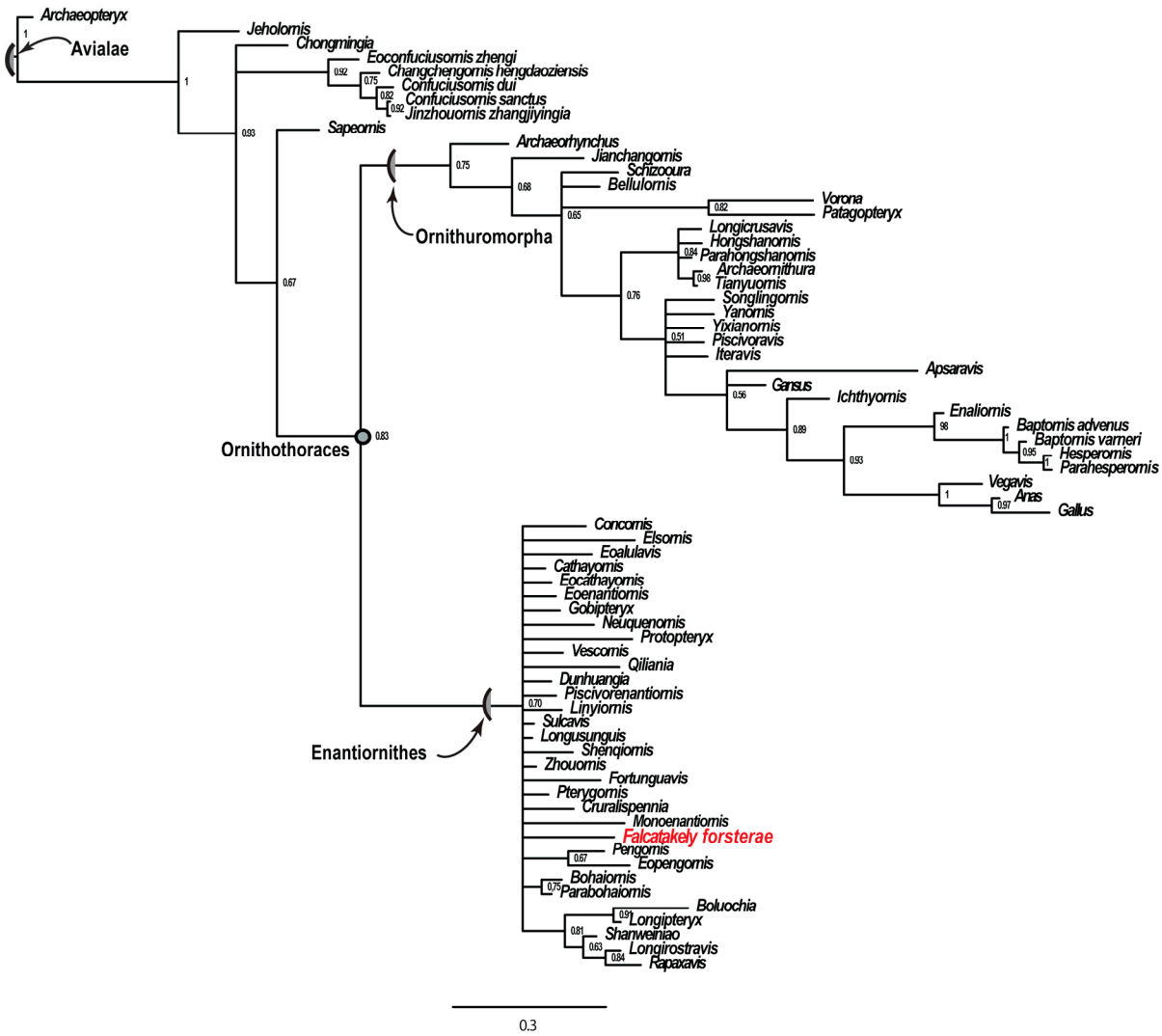

581

582 O’Connor et al. Extended Data Figure 4—Full-page width—Colour.

583

584

585

586

587

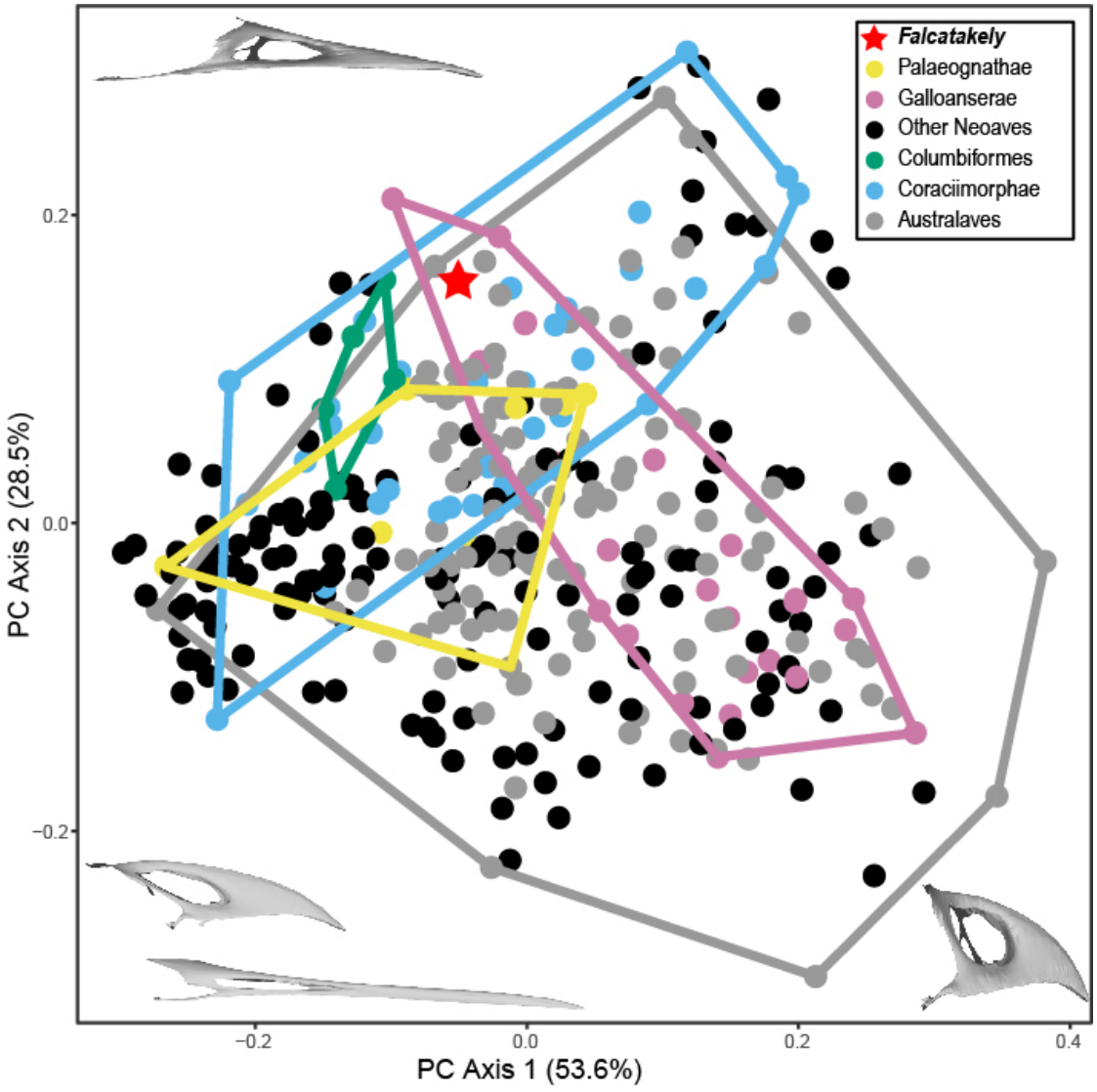

O'Connor et al. Extended Data Figure 5—1 ½ column width—Colour.

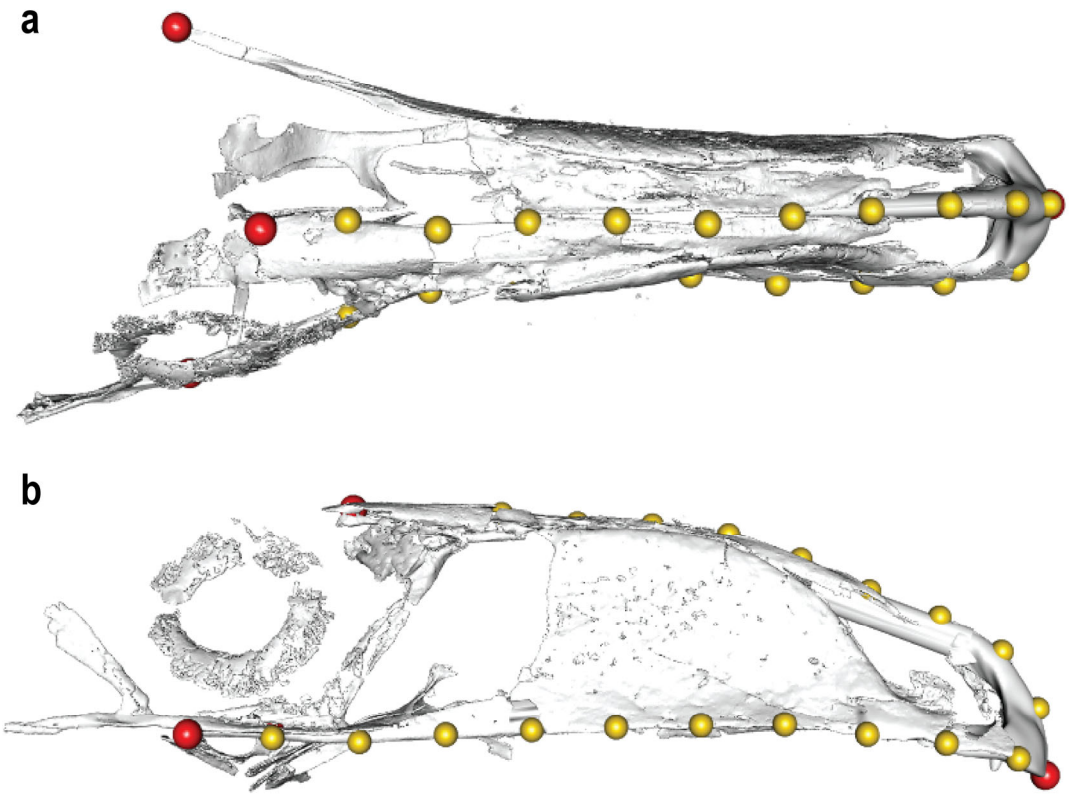

O'Connor et al. Extended Data Figure 6—column width—Colour.